Applied Mathematical Modelling 81 (2020) 372–385

Contents lists available at ScienceDirect

Applied Mathematical Modelling

journal homepage: www.elsevier.com/locate/apm

FPGA Realization of Fractional Order Neuron

S.A. Malik*, A.H. Mir

Machine Learning Lab, Electronics and Communication Department, National Institute of Technology, Srinagar, 190006, India

ARTICLE INFO

Article history:
Received 2 April 2019
Revised 1 December 2019
Accepted 9 December 2019
Available online 27 December 2019

Keywords:
Computational neuroscience
Fractional Hindmarsh Rose neuron (HR)
Fractional calculus
Fractional-operator
Field-programmable-gate-arrays (FPGA)
Synchronization

ABSTRACT

In this paper fractional Hindmarsh Rose (HR) neuron, which mimics several behaviors of a real biological neuron is implemented on field programmable gate array (FPGA). The results show several differences in the dynamic characteristics of integer and fractional order Hindmarsh Rose neuron models. The integer order model shows only one type of firing characteristics when the parameters of model remains same. The fractional order model depicts several dynamical behaviors even for the same parameters as the order of the fractional operator is varied. The firing frequency increases when the order of the fractional operator decreases. The fractional order is therefore key in determining the firing characteristics of biological neurons. To implement this neuron model first the digital realization of different fractional operator approximations are obtained, then the fractional integrator is used to obtain the low power and low cost hardware realization of fractional HR neuron. The fractional neuron model has been implemented on a low voltage and low power circuit and then compared with its integer counter part. The hardware is used to demonstrate the different dynamical behaviors of fractional HR neuron for different type of approximations obtained for fractional operator in this paper. A coupled network of fractional order HR neurons is also implemented. The results also show that synchronization between neurons increases as long as coupling factor keeps on increasing.

1. Introduction

MIMICKING the neuronal activity in the brain is the key focus in the field of computational neuroscience. To understand the different aspects of brain, computational neuroscience focuses on fundamental signaling unit-neurons and their interaction with one another in the nervous system [1,2]. This can be achieved by efficient mathematical models and numerical simulations of these neuronal units (both in software and hardware). This helps us to understand the functioning of our brain and thereby facilitate us in curing brain diseases, better design of robots, prosthetics and to study the fundamentals of artificial neural networks [2–5].

A neuron model is essentially a dynamic system that shows dynamical behavior, which can be described by a set of first order ordinary differential equations [6–9]. Several neuron models have been proposed in the last century which mimic the activities of some biological neurons with varying degree of biological accuracy. The most popular dynamical model of biological neuron is the Hodgkin-Huxley(HH) model [10], which describes the behaviour of membrane action potential of giant squid axon, by considering the ionic mechanism and current on the surface of the cell membrane. The other neuron

* Corresponding author.
E-mail address: shakeel_26phd17@nitsri.net (S.A. Malik).

https://doi.org/10.1016/j.apm.2019.12.008
0307-904X/

models include FitzHugh-Nagumo (FHN) model [11], Morris-Lecar model [12], Izhikevich model [5], Integrate-and-fire model (IF) [13], Leaky-Integrate-and-fire model [14].

The above-mentioned neuron dynamical models can be divided into two categories: firstly, conductance based models with high degree of biological accuracy but with high computational complexity and cost, such as HH model and secondly the simple spiking based models, which describe the spike and spike timings behavior of neurons such as IF model. On the other hand Hindmarsh-Rose (HR) model [15] is very simple mathematical model, which describes the thalmic neuron of brain and displays several real biological neuron behaviors and accurately models the frequency-stimulus current relationship. Recent studies [16–24] have shown that some already existing physical phenomena described by integer order calculus are more accurately described by their fractional counterparts. In [24] the dynamics of neocortical neuron are studied with a range of firing stimulus. The results showed that the neuron adapts to a time scale that depends on the time scale of changes in firing stimulus.The multiple time scale adaptation is consistent with fractional differentiation and therefore the firing rate of neocortical neuron is a fractional derivative of slowly varying stimulus parameter. Fractional derivative provides an excellent tool for depiction of memory properties. This is an important feature in modeling biological neurons [25], thus fractional derivative model has proved its supremacy over the other models viz a viz dynamics and wide range of functionalities. Recently there has been tremendous boost in the study and development of fractional order neuron models [26–30]. Recognizing the advantages of fractional order models, several researchers have attempted the circuit implementation of these fractional order models as circuit level implementation has several advantages compared to the software implementation [7,9,26]. One of the most prevalent advantages of hardware implementation is that these designs can perform the tasks much faster and can be physically connected with biological tissue to obtain the data in real time which boosts the design of robots. Although analog circuit implementation of fractional models and digital realization of integer order models already exits in the literature [28–32], no digital realization of these fractional neuron models exist in the literature to the best of our knowledge. Digital implementations although consume more silicon area and demand more power for each function as compared to analog realizations, however it's more robust to thermal noise and power supply fluctuations. Field programmable gate arrays (FPGAs) are digital reconfigurable devices that have less development time compared to analog and other digital devices [28,33,34]. In this paper we present FPGA implementation of fractional HR neuron as this neuron shows several dynamical behaviors of a real biological neuron and has mathematically less complexity compared with other biological neuron models. The main aim of this paper is to obtain the lost cost and low power realization of fractional HR neuron, that is achieved by first obtaining the realization of fractional operator in frequency domain and then this operator is used to obtain the discrete model of fractional HR neuron. The rest of the paper is organized as: section II presents a brief introduction to fractional order system, section III describes the different dynamical behaviors depicted by fractional HR neuron. Section IV describes the digital realization of fractional operator. Sections V and VI presents the hardware design and implementation results. Finally section VII concludes the paper.

2. Fractional order system

Fractional calculus is simply the generalization of integer order calculus to any real order. A physical phenomenon described by a fractional differential equation is given in equation (1)

$$ {}_{\nu}D_t^{\alpha} x = f(x) \tag{1}$$

where ν and t are respectively the lower and upper limits of fractional operator D, $\alpha \in \mathbb{R}$ is the order of operator D, $f \in \mathbb{R}^n$, $x \in \mathbb{R}^n (n \in \mathbb{N})$. Several definitions of the fractional operator exists in the literature but in continuous time domain Riemann-Liouville (RL) and Caputo definitions are mostly used [31,32]. These are given below

(1) RL fractional integral operator of order α is defined as:

$$ {}_0I_t^{\alpha}[f(t)] \equiv {}_0D_t^{-\alpha}[f(t)] = \frac{1}{\Gamma(\alpha)} \int_0^t \frac{f(\zeta)d\zeta}{(t-\zeta)^{1-\alpha}} \tag{2}$$

(2) Caputo derivative of order α is defined as:

$$ {}_0D_t^{\alpha}[f(t)] = \frac{1}{\Gamma(n-\alpha)} \int_0^t \frac{f^n(\zeta)d\zeta}{(t-\zeta)^{\alpha-n+1}} \tag{3}$$

where $n-1 < \alpha < n$, n is an integer, $\Gamma(.)$ is Eulers Gamma function, and f^n is nth derivative of $f(\zeta)$.The properties of these definitions are listed in [31,32].

Laplace transform is an important mathematical tool used to solve differential equations in science and engineering. Laplace transform of RL fractional integral in equation (2) as given in [32] is

$$ \mathcal{L}\{{}_0I_t^{\alpha}[f(t)]\} = s^{-\alpha}F(s) \tag{4}$$

Similarly the Laplace transform formula for Caputo fractional derivative in equation (3) is given in equation (4):

$$ \mathcal{L}\{{}_0D_t^{\alpha}[f(t)]\} = s^{\alpha}F(s) - \sum_{k=0}^{n-1} s^{\alpha-k-1} f^{(k)}(0) \tag{5}$$

where $f^k(0)$ denote the initial conditions of f(t). Neglecting these initial conditions we get

$$\mathcal{L}\{{}_0D_t^{\alpha}[f(t)]\} = s^{\alpha}F(s) \tag{6}$$

From (4) and (6) we get the definition of general differintegral fractional operator as:

$$\mathcal{L}\{{}_0D_t^{\pm\alpha}[f(t)]\} = s^{\pm\alpha}F(s) \tag{7}$$

In the section III we first show the digital realization of this fractional differintegral operator. The fractional HR neuron is a dynamical system [15] and has three coupled fractional differential equations as given below

$$\begin{aligned} D^{\alpha}x_1 &= x_2 - f_1(x_1) - x_3 + I \\ D^{\alpha}x_2 &= f_2(x_1) - x_2 \\ D^{\alpha}x_3 &= r(f_3(x_1) - x_3) \end{aligned} \tag{8}$$

where

$$\begin{cases} f_1(x_1) = ax_1^3 - bx_1^2 \\ f_2(x_1) = c - dx_1^2 \\ f_3(x_1) = s(x_1 + x_e) \end{cases} \tag{9}$$

where x_1 is the membrane potential variable, x_2 is the recovery current variable (also called spiking variable), x_3 is the adaptation variable (also known as bursting variable), I is the external applied current, x_e is the resting value of membrane potential x_1 and a,b,c,d,r and s are constants.

3. Fractional operator

The key step in hardware realization of fractional order systems requires proper discrete time forms of differ-integral operator $s^{\pm\alpha}$. This discrete time realization should be efficient, accurate and stable. In this section, we obtain the digital realization of differintegral operator obtained in section II and show its hardware implementation.

In general two discretization approaches are used: direct and indirect discretization. In the indirect approach the fractional operator is first approximated by continuous time finite order rational transfer function; i.e, $s^{\pm\alpha} \approx \frac{N(s,\alpha)}{D(s,\alpha)}$ and then the resulting continuous transfer function is discretized by replacing s by an appropriate discretized method such as Euler's method, bilinear (Tustin) transformation etc. Direct discretization approach involves the application of the direct power series expansion (PSE), continued fraction expansion (CFE), Maclaruin series expansion etc. of some proper conversion formulae [33–36]. In general, the discretization of fractional operator $s^{\pm\alpha}$ (where α is real) can be expressed by the generating function $s = H(z^{-1})$ which maps the continuous time operator to discrete time (s↔z). The commonly used generating functions include Bilinear, Simpson, Al-Alaoui, mixed Bilinear-Simpson, mixed Euler-Bilinear-Simpson, impulse response based and other higher order generating functions [37–39]. Some of these generating functions are listed below:

(i) Euler's Backward formula

$$H_E(z^{-1}) = \left[\frac{1 - z^{-1}}{T}\right]^{\pm\alpha} \tag{10}$$

where T is the sampling time.

(ii) Bilinear transformation

$$H_T(z^{-1}) = \left[\frac{2}{T}\cdot\frac{1 - z^{-1}}{1 + z^{-1}}\right]^{\pm\alpha} \tag{11}$$

(iii) Simpson's numerical integration formula

$$H_S(z^{-1}) = \left[\frac{3}{T}\cdot\frac{1 - z^{-2}}{1 - 4z^{-1} + z^{-2}}\right]^{\pm\alpha} \tag{12}$$

(iv) Al-Alaoui approximation which combines the trapezoidal(Tustin) formula and Euler's formula defines the transformations

$$s = \mu H_E(z^{-1}) + (1 - \mu)H_T(z^{-1}), \quad \mu \in [0, 1] \tag{13}$$

where μ is the tuning between Euler and trapezoidal rule. Using (5) and (6) in (7) we get the Al-Alaoui operator as

$$H_A(z^{-1}) = \left[\frac{T(1+\mu)}{2}\cdot\left(\frac{1 + \frac{(1+\mu)z^{-1}}{1-\mu}}{1 - z^{-1}}\right)\right]^{\pm\alpha} \tag{14}$$

In this paper we obtain the approximation of differintegral obtained by combining the frequency response of Euler and Tustin rule. The choice of this selection is guided by the fact that the magnitude starts rolling-off at higher frequencies if we only consider Tustin discretization. Therefore we combine the frequency response of Euler and Tustin to get a better realization of fractional integrator [38,39].

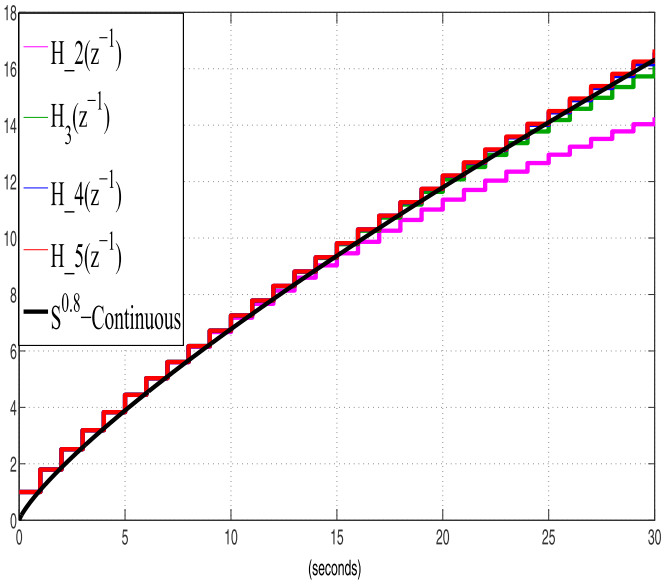

Fig. 1. Step response of fractional integrators for different approximations. The step response approaches to the continuous case as the number of terms in the approximation increases.

The above discretization approaches of $s^{\pm\alpha}$ may lead to finite impulse response (FIR) or infinite impulse response (IIR) form depending upon whether we use PSE or CFE expansion methods. The FIR form approximation of $s^{\pm\alpha}$ usually is less efficient due to the very high order of the FIR realization for same accuracy of IIR form. Also compared to the PSE method the CFE method of a function has faster and larger domain of convergence in the complex plain [34,36,37]. Therefore in this paper we consider only the CFE realization of $s^{\pm\alpha}$. The function $H(z^{-1})$ can be expressed in continued fraction as follows

$$H(z^{-1}) \approx a_0(z^{-1}) + \cfrac{b_0(z^{-1})}{a_1(z^{-1}) + \cfrac{b_1(z^{-1})}{a_2(z^{-1}) + \cfrac{b_2(z^{-1})}{a_3(z^{-1}) + \cfrac{b_3(z^{-1})}{a_4(z^{-1}) + \ldots}}}} \tag{15}$$

where the cofficients a_i's and b_i's are either rational functions of variable z^{-1} or simply constants. By truncating (18) and using different values of μ we get different approximations of the operator $s^{\pm\alpha}$. Some of the approximations are listed below for $\mu = 0$, T = 1 and $\alpha = -0.80$. In these results we write the approximation as $H_n(z^{-1})$, where n denotes the number of terms used in truncation

$$\begin{aligned}
H_2(z^{-1}) &= \frac{2.381 - 1.429z^{-1} + 0.04762z^{-2}}{2.381 - 3.333z^{-1} + z^{-2}} \\
H_3(z^{-1}) &= \frac{6.266 - 6.892z^{-1} + 1.654z^{-2} - 0.02757z^{-3}}{6.266 - 11.9z^{-1} + 6.667z^{-2} - z^{-3}} \\
H_4(z^{-1}) &= \frac{\left(\frac{18.27 - 29.24z^{-1} + 13.78z^{-2} -}{1.838z^{-3} + 0.01838z^{-4}}\right)}{\left(\frac{18.27 - 43.86z^{-1} + 35.71z^{-2}}{-11.11z^{-3} + z^{-4}}\right)} \\
H_5(z^{-1}) &= \frac{\left(\frac{56.72 - 119.1z^{-1} + 84.69z^{-2} -}{23.29z^{-3} + 1.996z^{-4} - 0.01331z^{-5}}\right)}{\left(\frac{56.72 - 164.5z^{-1} + 175.4z^{-2} -}{83.33z^{-3} + 16.67z^{-4} - z^{-5}}\right)}
\end{aligned} \tag{16}$$

The step response for these transfer functions is shown in Fig. 1. As shown in this figure higher the number of terms used in the CFE the response of discrete transfer function response approaches to the continuous response closely, which clearly requires more hardware. Therefore there is trade-off between accuracy and hardware cost for each approximation.

Now lets investigate the effect of tuning knob μ on the frequency response of these approximations. For this analysis we select third order approximation and vary the tunning parameter μ and set the sampling time T = 0.1. The approximations are denoted as $H_\mu(z^{-1})$, which are listed below.

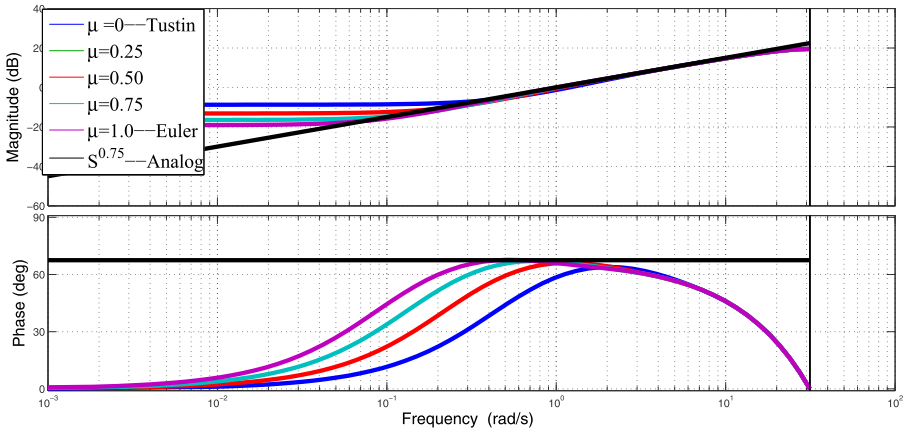

Fig. 2. BODE plot of fractional integrators obtained in (17). The response illustrates the use of tuning knob μ when sampling Time T = 0.1.

$$
\begin{aligned}
H_{0.00}(z^{-1}) &= \frac{959.7 - 1799z^{-1} + 989.7z^{-2} - 144.3z^{-3}}{170.7 - 192z^{-1} + 48z^{-2} - z^{-3}} \\
H_{0.25}(z^{-1}) &= \frac{254.2 - 405.1z^{-1} + 159.4z^{-2} - 5.531z^{-3}}{38.24 - 25.09z^{-1} - 2.912z^{-2} + z^{-3}} \\
H_{0.50}(z^{-1}) &= \frac{3.122e04 - 4.098e04z^{-1} + 8049z^{-2} + 2325z^{-3}}{4096 - 768z^{-1} - 1248z^{-2} - z^{-3}} \\
H_{0.75}(z^{-1}) &= \frac{120.6 - 124.4z^{-1} - 9.185z^{-2} + 16.74z^{-3}}{14.09 + 3.964z^{-1} - 5.698z^{-2} - z^{-3}} \\
H_{1.00}(z^{-1}) &= \frac{55.02 - 41.27z^{-1} - 20.63z^{-2} + 9.457z^{-3}}{5.818 + 4.364z^{-1} - 2.182z^{-2} - z^{-3}}
\end{aligned} \tag{17}
$$

similarly we get impact of tunning knob μ when sampling time T = 0.0001, as follows.

$$
\begin{aligned}
H_{0.00}(z^{-1}) &= \frac{\left(\frac{1.707e05 - 320000z^{-1} + 176000z^{-2}}{-2.567e04z^{-3}}\right)}{170.7 - 192z^{-1} + 48z^{-2} - z^{-3}} \\
H_{0.25}(z^{-1}) &= \frac{\left(\frac{4.52e04 - 7.204e041z^{-1} + 2.834e04z^{-2}}{-983.5z^{-3}}\right)}{38.24 - 25.09z^{-1} - 2.912z^{-2} + z^{-3}} \\
H_{0.50}(z^{-1}) &= \frac{\left(\frac{5.552e06 - 7.287e06z^{-1} + 1.431e06z^{-2}}{+4.134e05z^{-3}}\right)}{4096 - 768z^{-1} - 1248z^{-2} - z^{-3}} \\
H_{0.75}(z^{-1}) &= \frac{\left(\frac{2.144e04 - 2.211e04z^{-1} - 1633z^{-2}}{+2977z^{-3}}\right)}{14.09 + 3.964z^{-1} - 5.698z^{-2} - z^{-3}} \\
H_{1.00}(z^{-1}) &= \frac{9785 - 7339z^{-1} - 3669z^{-2} + 1682z^{-3}}{5.818 + 4.364z^{-1} - 2.182z^{-2} - z^{-3}}
\end{aligned} \tag{18}
$$

The Bode plot of results in (17) and (18) are shown in Figs. 2 and 3 respectively. As shown, if Tustin operator ($\mu = 1$) is used the high frequency response of this approximation completely differ from the ideal continuous time case, which shows that the role of tuning knob μ is useful for some applications as illustrated in Figs. 2 and 3.

Above approximations of the fractional operator can be realized in discrete hardware by using various approaches such as direct form I, direct form II etc. However as direct form II requires less resources as compared to direct form I, therefore we realize the approximation by using direct form II structure [34]. The difference equation corresponding to 2nd order realization is given below.

$$
y(n) = \frac{1}{a_1}\left(b_1x(n) + b_2x(n-1) + b_3x(n-2) - a_2y(n-1) - a_3y(n-2)\right) \tag{19}
$$

4. Dynamics of fractional order HR neuron

The transition from equilibrium state to the unstable state of a dynamical system is controlled by its parameters [40–42]. Therefore the stability analysis of a non-linear dynamical system requires thorough investigation of different parameter combinations of a non-linear model.

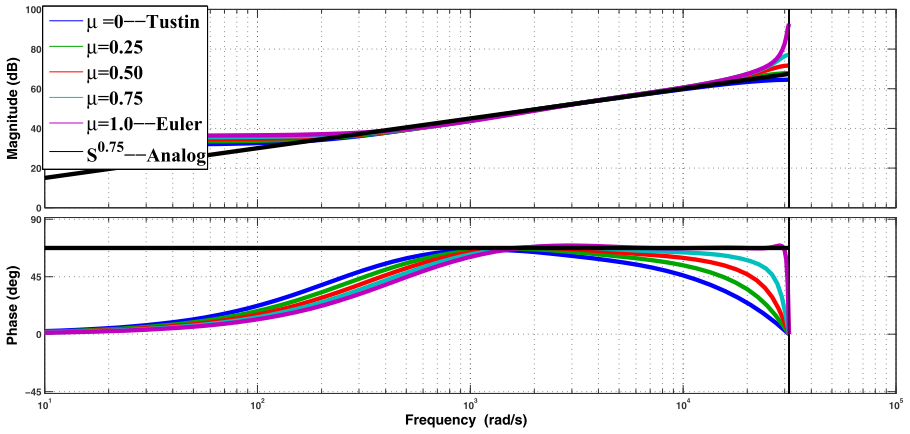

Fig. 3. BODE plot of fractional integrators obtained in (18). The response illustrates the use of tuning knob μ when sampling Time T = 0.0001.

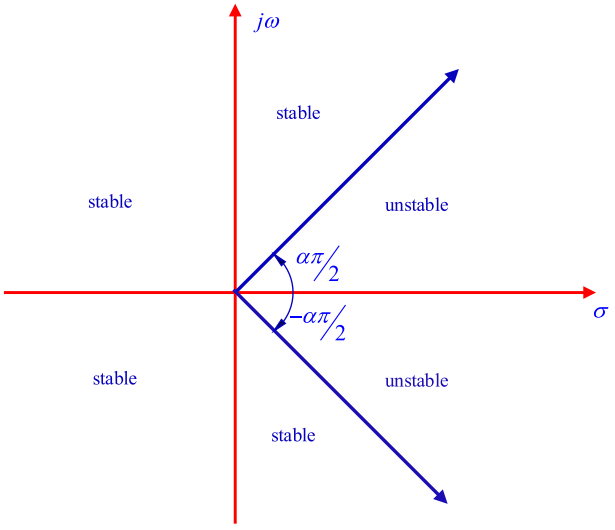

Fig. 4. Stable region of the linear fractional order (α) system when $0 < \alpha < 1$.

The stability analysis of linear fractional order autonomous system is given in [42,43]. A linear fractional order system is given as:

$$ {}_0D_t^{\alpha} x = Ax \quad and \quad x(0) = x_0 \tag{20} $$

where x $\in$ $\mathbb{R}^n$ and A $\in$ $\mathbb{R}^{n\times n}$ is an n x n matrix, ($n \in \mathbb{N}$). Let λ be the eigenvalues of matrix A.

(i) Linear system (20) is asymptotically stable if and only if $|arg(\lambda)| > \frac{\alpha\pi}{2}$.
(ii) Linear system (20) is stable if and only if $|arg(\lambda)| \geq \frac{\alpha\pi}{2}$ is satisfied for all eigenvalues of the matrix A with critical eigenvalue $|arg(\lambda)| = \frac{\alpha\pi}{2}$ having periodic dynamic behaviour. The stable regoin of a fractional order system is shown in Fig. 4.

As mentioned in equation (8), the HR fractional order neuron has three coupled non-linear fractional differential equations. For stability analysis and firing properties of above neuron we will treat I, r and α as variables. In general fractional HR neuron exhibits three kinds of behaviours:(i) spiking (ii) bursting, and (iii) chaotic.

Suppose that (x_1^*, x_2^*, x_3^*) is the equilibrium point of HR neuron (8). The jacobian J of HR neuron (8) at point (x_1^*, x_2^*, x_3^*) is given as

$$ J = \begin{bmatrix} 2bx_1^* - 3ax_1^{*2} & 1 & -1 \\ -2dx_1^* & -1 & 0 \\ rs & 0 & -r \end{bmatrix} \tag{21} $$

Let the eigenvalues of (11) are λ_1, λ_2, λ_3, then the stability of the equilibrium point (x_1^*, x_2^*, x_3^*) is defined as:

(1) if $|arg(\lambda_i)| > \frac{\pi}{2}$, then the equilibrium point (x_1^*, x_2^*, x_3^*) is locally asymptotically stable.

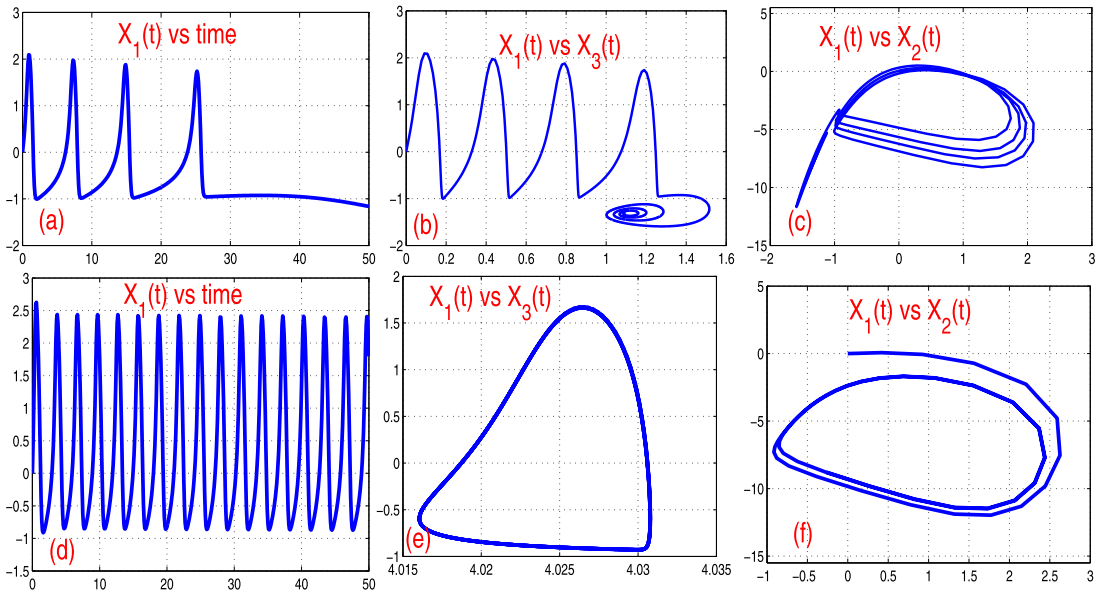

Fig. 5. Transition from resting to spiking state of integer order HR when a = 1,b = 3,c = 1,d = 5,s = 4,r = 0.001 and variable stimulus current I. (a) Resting state when I = 1.2 $\alpha = 1$, (b) $X_1(t)$ & $X_3(t)$ Phase space trajectory for $\alpha = 1$ I = 1.20, (c) $X_1(t)$ & $X_2(t)$ Phase space trajectory for $\alpha = 1$ I = 1.20 (d) Peridic spiking I = 4 $\alpha = 1$, (e) $X_1(t)$ & $X_3(t)$ Phase space-stable limit cycle trajectory for $\alpha = 1$ I = 4 (f) $X_1(t)$ & $X_2(t)$ Phase space trajectory for $\alpha = 1$ I = 4.

(2) if $|arg(\lambda_i)| \geq \frac{\pi}{2}$, then the equilibrium point (x_1^*, x_2^*, x_3^*) is locally stable.
(3) If $|arg(\lambda_i)| < \frac{\pi}{2}$,then the equlilibrium point (x_1^*, x_2^*, x_3^*) is unstable, where i = 1,2,3.

The transition from resting state to the spiking state of equilibrium point (x_1^*, x_2^*, x_3^*) of (8) is controlled by these parameters r, α and I. When $\alpha = 1$ the fractional HR neuron becomes ordinary HR neuron.

When a = 1,b = 3,c = 1,d = 5,s = 4,x_e=−1.6, r = 0.001 then all the eigenvalues of (21) have negative real part for $0 < I < 1.26$. Therefore $|arg(\lambda_i)| > \frac{\alpha\pi}{2}$, for $0 < \alpha \leq 1$. Hence the equilibrium point is locally stable for any value of fraction α. When $I > 1.26$ the eigenvalues of Jacobian matrix (21) have positive real part at the equilibrium point (x_1^*, x_2^*, x_3^*) and then $|arg(\lambda_i)| < \frac{\alpha\pi}{2}$ for $0 < \alpha \leq 1$. Therefore the equilibrium point is locally unstable. This is shown in figures (5) and (6) for both the integer and fractional order cases respectively. As the value of stimulus current increases, the phase space approaches to a stable limit cycle. The trajectory approaches to a stable limit cycle for different values of I in integer and fractional order HR neuron and the neuron fires periodically depicts the spiking behavior. This is illustrated in the phase space diagrams in figures 6(e), 6(f) and figure 7(e), 7(f) respectively.

For the integer order HR neuron the equilibrium point is unstable when $I > 1.26$, but it may be locally stable for the fractional order HR neuron. To illustrate this consider I = 1.30, then the equilibrium point of (8) is (−1.3212,−7.7282,1.1151), the eigenvalues of (11) are: $\lambda_1 = -14.1674$, $\lambda_2 = 0.0011 + 0.0167i$ and $\lambda_3 = 0.0011 - 0.0167i$. Therefore, $|arg(\lambda_1)| = \pi$, $|arg(\lambda_2)| = 1.5050$ and $|arg(\lambda_3)| = 1.5050$. From the stability criteria mention above, the point is locally stable if $\alpha < 1.5050.\frac{2}{\pi} = .9581$ and the equilibrium point is unstable when $\alpha > .9581$. This is illustrated in figure 7(d) where the membrane potential approaches to the resting value after sometime. Figure 7(e) shows the limit cycle for $\alpha = 0.9$, when I = 1.5 and the fractional HR neuron displays periodic spiking behaviour.

The bifurcation study of Integer order HR neuron has already been carried out in [44,45]. In our bifurcation study we treat α as a variable and study its impact on its dynamical behavior. Nemerical simulations shows that for different values of order the HR neuron displays different types of bursting behaviors. The integer order HR neuron shows chaotic behavior at I = 3.0,b = 2.96, when other parameters are kept same as given above. The fractional neuron may exhibits the same behavior for different values of parameters choosen above. Nemerical simulations shows that for different values of order the HR neuron displays different types of bursting behaviors. As shown in Fig. 7 above the HR neuron shows chaotic bursting at $\alpha = 0.95$, period 1 burst for $\alpha = 0.9$, period 2 burst when $\alpha = 0.88$. The frequency of bursting pattern increases as the order of the fractional neuron decreases. Therefore the bifurcation properties can be controlled by the fractional order (α) also, thus giving us another degree of freedom for dynamical analysis for HR neuron. Numerical simulations show that the bursting pattern depends on the parameters I and r. This is illustrated in Fig. 8. For both the integer and fractional neuron the bursting characteristics change with these parameters. The bursting frequency increases as r increases and the number of spikes in each burst is changing with I.

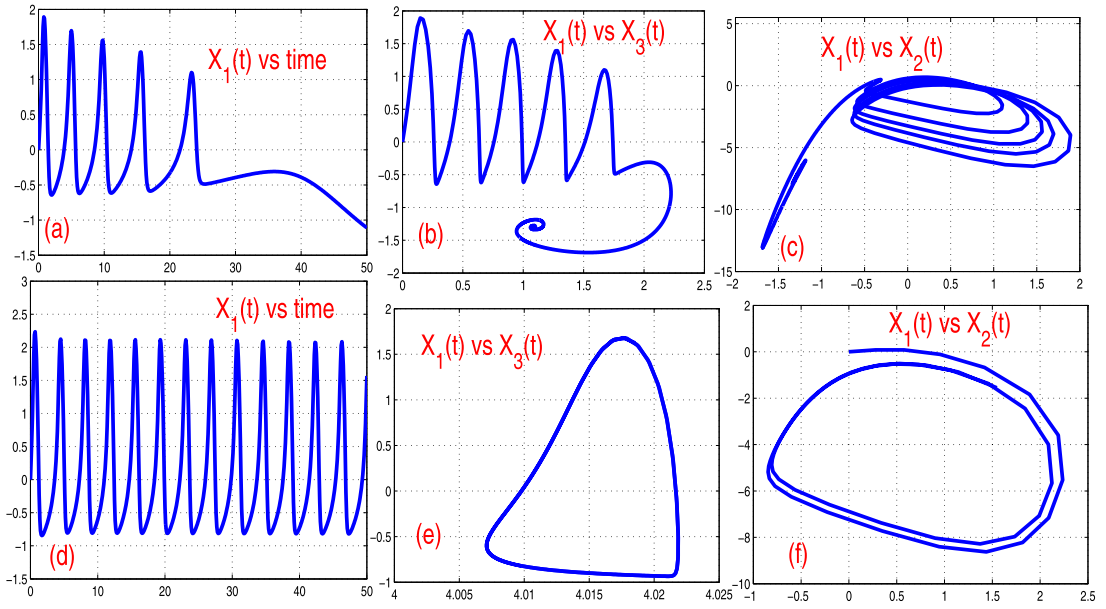

Fig. 6. Transition from resting to spiking state of integer order HR when a = 1,b = 3,c = 1,d = 5,s = 4,r = 0.001 and variable stimulus current I. (a) Resting state when I = 1.2 $\alpha = 0.9$, (b) $X_1(t)$ & $X_3(t)$ Phase space trajectory for $\alpha = 0.9$, I = 1.20, (c) $X_1(t)$ & $X_2(t)$ Phase space trajectory for $\alpha = 0.9$ I = 1.20 (d) Peridic spiking for I = 1.5, $\alpha = 0.9$, (e) $X_1(t)$ & $X_3(t)$ Phase space-stable limit cycle trajectory for $\alpha = 0.9$, I = 1.5 (f) $X_1(t)$ & $X_2(t)$ Phase space trajectory for $\alpha = 0.9$, I = 1.5.

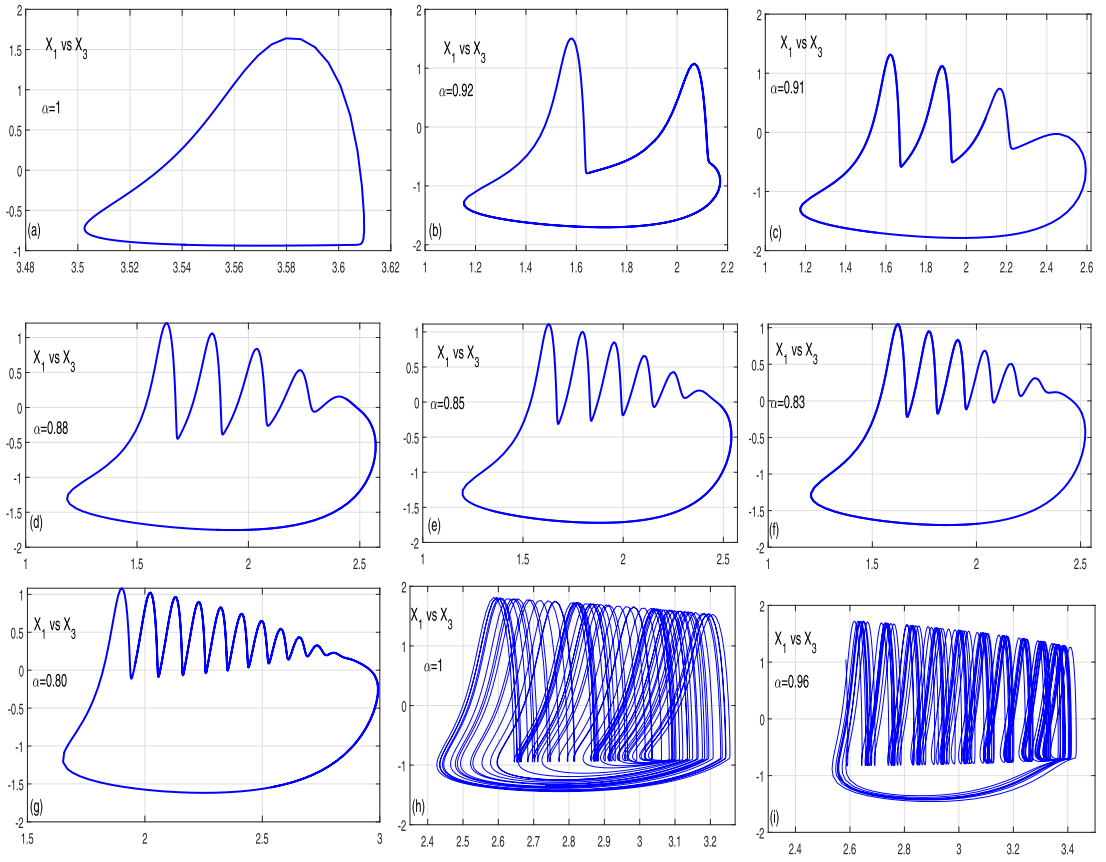

Fig. 7. Bursting pattern characteristics for different values of α when a = 1,b = 3,c = 1,d = 5,s = 4, Bursting frequency increases as α decreases(a) Period one burst at $\alpha = 0.9$, (b) Period two burst at $\alpha = 0.88$,(c) Multi-bursting at $\alpha = 0.75$ and (d) Chaotic burst at $\alpha = 1$ and $\alpha = 0.95$ in (h) and (i) respectively.

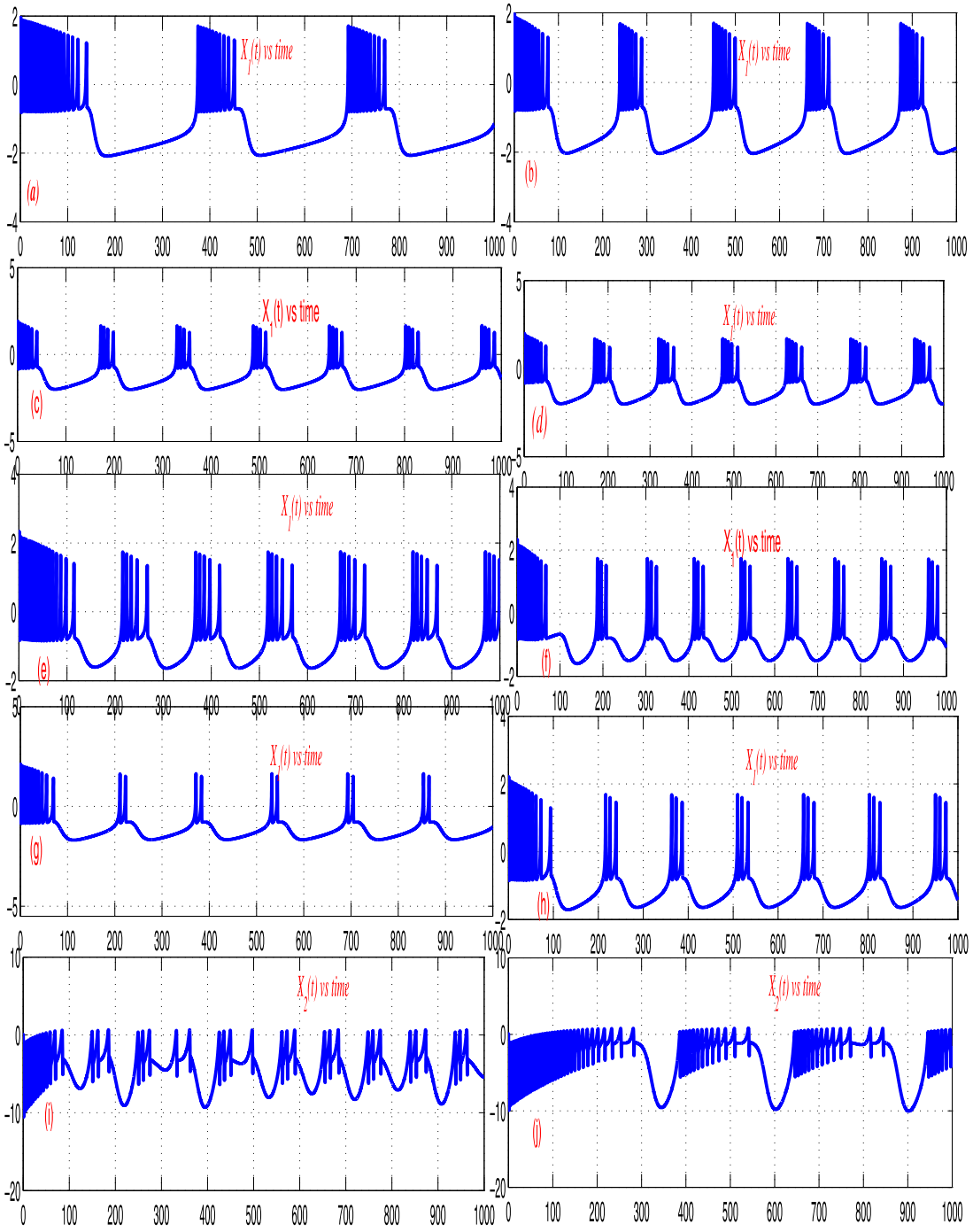

Fig. 8. Bursting characteristics for different values of I and r, when a = 1,b = 2.7,c = 1,d = 5,s = 4.Number of bursts increases as the value of bursting parameter r increases from r = 0.001 to 0.006 in (a) to (b) respectively. Number of spikes increases in burst as input stimulus I increases 1.6 to 1.9 in (c) to (d) respectively. Frequency of burst increases as r increases from 0.003 to 0.005 in (e) to (f) respectively. Both r and I increase from r = 0.002, I = 1.4 to r = 0.006, I = 1.6 in (g) to (h) respectively. (i) shows recovery current under chaotic behaviour when $\alpha = 1$ (j) shows the recovery current variable under chaotic behaviour.

5. Coupling of fractional HR neurons

In this section, primarily dynamical behavior of two coupled fractional order Hindmarsh Rose (HR) neurons are presented. The communication in biological neurons in brain occurs through synaptic connection called as synapses between the two neurons. The signal that a neuron receives from the other neurons travels through this synaptic connection between them

Table 1
MAE computations for different values of coupling factor with fractional integrator of order $\alpha = 0.9$.

C_i	MAE_{RS} $x_{pre1} - x_{post1}$	MAE_{SS} $x_{pre1} - x_{post1}$	MAE_{BS} $x_{pre1} - x_{post1}$
−3.0	1.2092	2.5476	2.6527
−2.0	1.1832	2.5136	2.6462
−1.0	1.1449	2.4420	2.6167
−0.5	1.1006	2.3954	2.5732
0.5	0.6936	0.9865	0.8892
1.0	0.0572	0.0863	0.0656
2.0	0.0327	0.0652	0.0432
3.0	0.0224	0.0456	0.0345
4.0	0.0067	0.0089	0.0073
5.0	0.0023	0.0035	0.0039

Abbreviations: MAE_{RS} (Mean absolute error for resting state), MAE_{SS} (Mean absolute error for spiking state), MAE_{BS} (Mean absolute error for bursting state)
n is taken as 8000 in each calculution of MAE.

that depends upon the threshold value of the voltage level of the presynaptic neuron. Therefore the synaptic connection acts as a gate between two neurons. The synaptic junction can be modeled as coupling function between different neurons in the brain. When the value of the presynaptic voltage reaches to the threshold value, voltage transmission takes place through the synaptic connection between two neurons [1–5]. The synchronization of neuronal architectures play a very significant role for the processing of biological signals and play important role for the study and understanding of fundamental architecture of biological brain. The coupled network based on fractional order HR neuron has all the parameters of single HR neuron and the coupling function. Therefore, the synchronization and the dynamics of coupled HR neuron system can be controlled by that parameters I, r, b, α and the synaptic function.

The coupled model is specified as follows:

$$\begin{aligned}
\frac{d^\alpha x_{pre1}}{dt^\alpha} &= x_{pre2} - x_{pre3} + f_1(x_{pre1}) + g(x_{pre1}, x_{post1}) \\
\frac{d^\alpha x_{pre2}}{dt^\alpha} &= c - dx_{pre1}^2 - x_{pre2} \\
\frac{d^\alpha x_{pre3}}{dt^\alpha} &= r(s(x_{pre1} + x_e) - x_{pre3}) \\
\frac{d^\alpha x_{post1}}{dt^\alpha} &= x_{post2} - x_{post3} + f_2(x_{post1}) + g(x_{pre1}, x_{post1}) \\
\frac{d^\alpha x_{post2}}{dt^\alpha} &= c - dx_{post1}^2 - x_{post2} \\
\frac{d^\alpha x_{post3}}{dt^\alpha} &= r(s(x_{post1} + x_e) - x_{post3})
\end{aligned} \tag{22}$$

where

$$\begin{cases}
f_1(x_{pre1}) = I - ax_{pre1}^3 + bx_{pre1}^2 + a_1 cos(2\pi f_1 t) \\
f_1(x_{post1}) = I - ax_{post1}^3 + bx_{post1}^2 + a_2 cos(2\pi f_2 t)
\end{cases} \tag{23}$$

where x_{pre1} and x_{post1} respectively denote the membrane potential of presynaptic and postsynaptic neurons, x_{pre2} and x_{post2} denotes the spiking current variables of pre and post-synaptic neurons, similarly x_{pre3} and x_{post3} are pre and post-synaptic neuron bursting variables and $g(x_{pre1}, x_{post1})$ is the coupling function. In this coupling we have added two sinusoidal sources to evaluate the effectiveness and robustness of the proposed control scheme for all time. These two sinusoidal noise perturbations of high frequency is used to simulate the ionic channel noise of neurons, which is actually the most common disturbances in computational neuroscience. Here we assume the coupling function is linear and is defined as:

$$g(x_{pre1}, x_{post1}) = C(x_{pre1} - x_{post1}) \tag{24}$$

where C is the coupling factor.

Fig. 9 shows the different behaviors of two fractional order coupled neuron for different values of coupling factor. In all the cases the synchronization between neurons increases as the value of coupling factor increases. Each figure in (9) shows the phase space curve for presynaptic and postsynaptic neurons. The synchronization increases as the value of coupling increases which can be seen in Fig. 10 and Table 1. Fig. 10 and Fig. 11 shows that the absolute error of potentials of two neurons decreases as the value of coupling factor increases from −3 to 5.

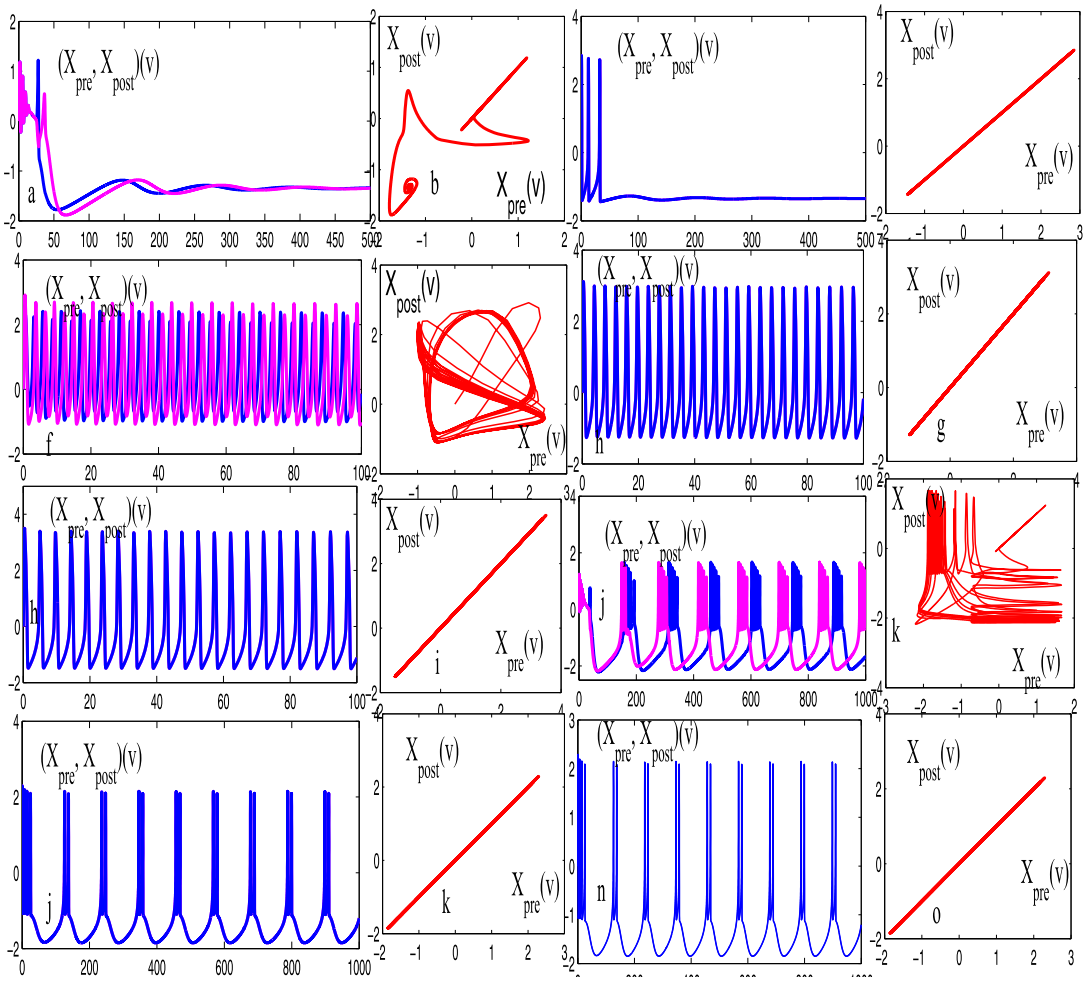

Fig. 9. Synchronization characteristics of two fractional HR neurons in Resting, Spiking and Bursting states when $\alpha = 0.80$. Unsynchronized at C=−0.5 and synchronization increases as the value of C increases from 0.5 to 5 as shown in the phase space diagrams.

Table 2
Resource utilization of the altera DE2-115 board.

INTO						
Res.	1	2	3	4	5	Avi
LEs.	3825	5349	6783	8229	9540	114480
Util.	3%	5%	6%	7%	8%	
Reg.	3455	4823	6089	7367	8636	114480
Util.	3%	4%	5%	6%	8%	
Mul.	12	12	12	12	12	266
Util.	4%	4%	4%	4%	4%	
Mb	0	0	0	0	0	3981312
Util	0%	0%	0%	0%	0%	
Po	316.5	344.35	367.31	387.33	419.25	1.2
Use.	mW	mW	mW	mW	mW	V
Fre.	100	100	100	100	100	Hz
FPAA	FPAA-1	128 ± 38 mW		Ref.		± 2
Version	FPAA-2	56 ± 17 mW		[26]		V
CMOS	Analog Design	112 nW		Ref.		± 0.65
Based				[27]		V

Abbreviations: RES(Resource name), UTIL (Percentage of resource utilization), LEs (Logic elements), MB (Memory bits used),AVI (Total availaible resouces), MUL(18 x 18s Multipliers used), INTO(Order of integrator used), Po. Use.(Power used), Fre.(Frequency).

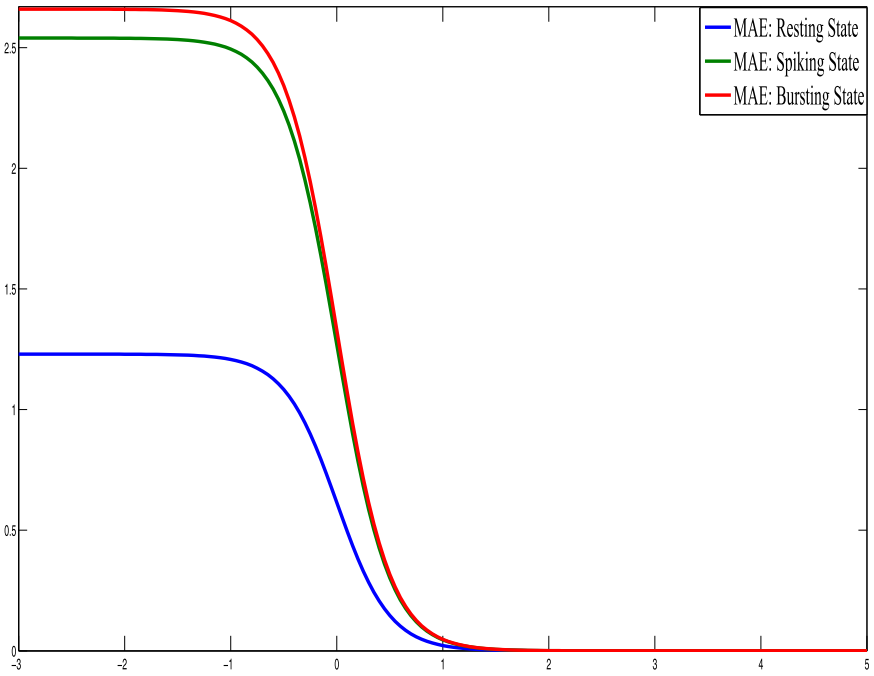

Fig. 10. Mean absolute error in Resting state, Bursting State and Spiking state of two fractional order neurons. The synchronization error decreases as the value of coupling factor increases.

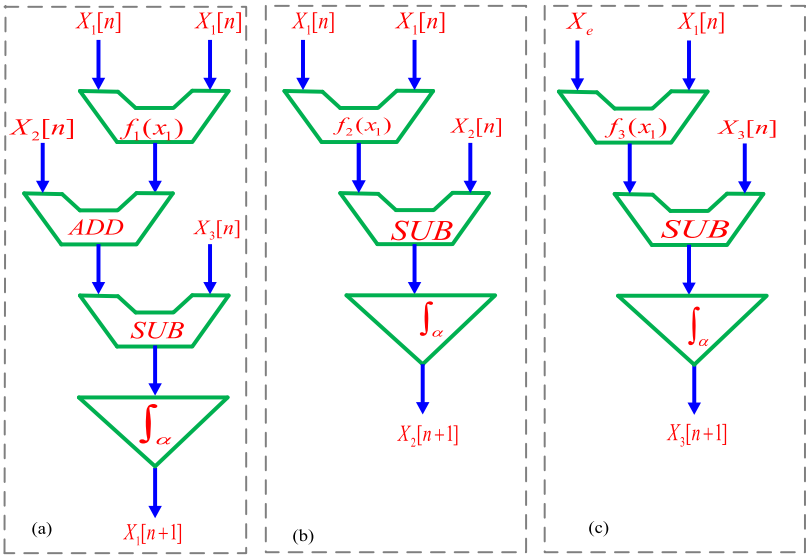

Fig. 11. The flow diagram of fractional HR neuron (a) The membrane potential $x_1(n)$ (b) The Spiking variable $x_2(n)$ (c) The adaptation variable $x_3(n)$, Fractional Integrator($\int_\alpha$).

6. Hardware Design

In this section we present the hardware implementation of fractional HR neuron. The first step in the hardware realization is to obtain the discrete realization of the given model. To obtain the hardware design we use the fractional integrators presented in section (III) above. The second step is to determine the number of bits for the signal generated in the model. As seen from above the maximum span of the membrane potential is from −2.5 to 2.5, therefore 3 bits are required to represent the membrane potential. However, an overflow due to the function $f_1(x_1)$, $f_2(x_1)$, $f_3(x_1)$ and due to coupling function multipliers can occur. To increase the accuracy of calculations and avoid any overflow, a bit width of 32 that consists of 8 bit integer part and 24 bit fractional part is considered. The rationale behind the utilization of more bits is to achieve a

better representation of floating point values. Also to represent the fractional part of the values more accurately we use 32 bit fixed width, as fixed point has less cost and complexity compared to floating point. In this 8 bits will be assigned to integer part and 24 will be used for fractional part. The flow diagram of hardware is shown in the Fig. 11.

7. Implementation results

Altera DE2-115 circuit board is used for the implementation of above model. As seen above to obtain accurate digital approximation of fractional integrator more hardware is needed. Therefore more accurate the approximation more the hardware resource utilization in the realization.Hence there is trade off between the accuracy and resource utilization for fractional modeling of HR neuron. The resource utilization of above model is summarized in Table 2 for different integrator approximations.

Conclusion

A low cost hardware implementation of fractional Hindmarsh Rose (HR) neuron is implemented in this paper. The hardware results demonstrate several dynamical behaviors depicted by this fractional neuron, which can also be controlled by the order of the fraction used in the neuron model. The bursting frequency increases as the order of fraction decreases. The accuracy of the digital realization of the fractional operator increases as the number of terms used in the approximation increases which also increases the hardware and power consumption. Therefore there is trade-off between accuracy and resource usage of fractional order HR neuron. A coupled fractional order system is also implemented in presence of noise. The two neurons were coupled using a linear coupling function. The synchronization between two neurons increases as the coupling factor increases, thereby decreasing the mean absolute error (MAE) between the membrane potentials of the two neurons. The dynamic behavior produced by this network depends upon the parameter values of HR model, current stimulus and coupling parameters, producing different patterns of bursting, spiking and chaotic behaviors with minimum computational error.

References

[1] P. Dayan, L.F. Abbott, Theoretical neuroscience: computational and mathematical modeling of neural systems, J. Cognit. Neurosci., MIT Press 15 (1) (2003) 154–155.
[2] E.M. Izhikevich, Dynamical Systems in Neuroscience, MIT Press, 2007.
[3] S.K. Talwar, S. Xu, E.S. Hawley, S.A. Weiss, K.A. Moxon, J.K. Chapin, Behavioural neuroscience: rat navigation guided by remote control, Nature 417 (6884) (2002) 37.
[4] G. Schöner, Dynamical systems approaches to cognition, in: Cambridge Handbook of Computational Cognitive Modeling, 2008, pp. 101–126.
[5] E.M. Izhikevich, Simple model of spiking neurons, IEEE Trans. Neural Netw. 14 (6) (2003) 1569–1572.
[6] S. Ching, E.N. Brown, Modeling the dynamical effects of anesthesia on brain circuits, Curr. Opin. Neurobiol. 25 (2014) 116–122.
[7] T. Yu, G. Cauwenberghs, Analog vlsi biophysical neurons and synapses with programmable membrane channel kinetics, IEEE Trans. Biomed. Circuit. Syst. 4 (3) (2010) 139–148.
[8] W. Wang, G. Perez, H.A. Cerdeira, Dynamical behavior of the firings in a coupled neuronal system, Phys. Rev. E 47 (4) (1993) 2893.
[9] P. Gao, B.V. Benjamin, K. Boahen, Dynamical system guided mapping of quantitative neuronal models onto neuromorphic hardware, IEEE Trans. Circuit. Syst. I 59 (10) (2012) 2383–2394.
[10] A.L. Hodgkin, A.F. Huxley, A quantitative description of membrane current and its application to conduction and excitation in nerve, J. Physiol. 117 (4) (1952) 500–544.
[11] R. FitzHugh, Impulses and physiological states in theoretical models of nerve membrane, Biophys. J. 1 (6) (1961) 445–466.
[12] C. Morris, H. Lecar, Voltage oscillations in the barnacle giant muscle fiber, Biophys. J. 35 (1) (1981) 193–213.
[13] L.F. Abbott, Lapicques introduction of the integrate-and-fire model neuron (1907), Brain Res. Bull. 50 (5–6) (1999) 303–304.
[14] Y.-H. Liu, X.-J. Wang, Spike-frequency adaptation of a generalized leaky integrate-and-fire model neuron, J. Comput. Neurosci. 10 (1) (2001) 25–45.
[15] R. Rose, J. Hindmarsh, The assembly of ionic currents in a thalamic neuron. ii. the stability and state diagrams, Proc. R. Soc. Lond. B 237 (1288) (1989) 289–312.
[16] R. Hilfer, et al., Applications of Fractional Calculus in Physics, 35, World Scientific, 2000.
[17] R.L. Magin, Fractional Calculus in Bioengineering, Begell House Redding, 2006.
[18] D. Baleanu, Z.B. Güvenç, J.T. Machado, et al., New Trends in Nanotechnology and Fractional Calculus Applications, Springer, 2010.
[19] M.D. Ortigueira, An introduction to the fractional continuous-time linear systems: the 21st century systems, IEEE Circuit. Syst. Mag. 8 (3) (2008).
[20] T.J. Anastasio, The fractional-order dynamics of brainstem vestibulo-oculomotor neurons, Biol. Cybernet. 72 (1) (1994) 69–79.
[21] R.L. Magin, Fractional calculus models of complex dynamics in biological tissues, Comput. Math. Appl. 59 (5) (2010) 1586–1593.
[22] A. Nagy, N. Sweilam, An efficient method for solving fractional Hodgkin–Huxley model, Phys. Lett. A 378 (30–31) (2014) 1980–1984.
[23] E. Kaslik, S. Sivasundaram, Nonlinear dynamics and chaos in fractional-order neural networks, Neural Netw. 32 (2012) 245–256.
[24] B.N. Lundstrom, M.H. Higgs, W.J. Spain, A.L. Fairhall, Fractional differentiation by neocortical pyramidal neurons, Nat. Neurosci. 11 (11) (2008) 1335.
[25] H. Sun, W. Chen, H. Wei, Y. Chen, A comparative study of constant-order and variable-order fractional models in characterizing memory property of systems, Eur. Phys. J. Spec. Top. 193 (1) (2011) 185.
[26] N. Dahasert, İ. Öztürk, R. Kiliç, Experimental realizations of the hr neuron model with programmable hardware and synchronization applications, Nonlinear Dyn. 70 (4) (2012) 2343–2358.
[27] F.A. Khanday, M.R. Dar, N.A. Kant, J.L. Rossello, C. Psychalinos, 0.65 V integrable electronic realisation of integer-and fractional-order hindmarsh–rose neuron model using companding technique, IET Circuits, Devices & Systems 12 (6) (2018) 696–706.
[28] M. Hayati, M. Nouri, D. Abbott, S. Haghiri, Digital multiplierless realization of two-coupled biological hindmarsh–rose neuron model, IEEE Trans. Circuit. Syst. I 63 (5) (2016) 463–467.
[29] N. Dahasert, İ. Öztürk, R. Kiliç, Experimental realizations of the HR neuron model with programmable hardware and synchronization applications, Nonlinear Dyn. 70 (4) (2012) 2343–2358.
[30] A.S. Elwakil, Fractional-order circuits and systems: an emerging interdisciplinary research area, IEEE Circuit. Syst. Mag. 10 (4) (2010) 40–50.
[31] I. Podlubny, Fractional Differential Equations: An Introduction to Fractional Derivatives, Fractional Differential Equations, to Methods of Their Solution and Some of Their Applications, 198, Elsevier, 1998.
[32] I. Petráš, Fractional-Order Nonlinear Systems: Modeling, Analysis and Simulation, Springer Science & Business Media, 2011.

[33] Y.Q. Chen, K.L. Moore, Discretization schemes for fractional-order differentiators and integrators, IEEE Trans. Circuit. Syst. I 49 (3) (2002) 363–367.
[34] B. Vinagre, I. Petras, P. Merchan, L. Dorcak, Two digital realizations of fractional controllers: Application to temperature control of a solid, in: Control Conference (ECC), 2001 European, IEEE, 2001, pp. 1764–1767.
[35] A. Oustaloup, F. Levron, B. Mathieu, F.M. Nanot, Frequency-band complex noninteger differentiator: characterization and synthesis, IEEE Trans. Circuit. Syst. I 47 (1) (2000) 25–39.
[36] A. Oustaloup, Fractional order sinusoidal oscillators: optimization and their use in highly linear fm modulation, IEEE Trans. Circu. Syst. 28 (10) (1981) 1007–1009.
[37] M.A. Al-Alaoui, Novel digital integrator and differentiator, Electron. Lett. 29 (4) (1993) 376–378.
[38] A.A. Mohamad Adnan, Filling the gap between the bilinear and the backward-difference transforms: an interactive design approach, Int. J. Electr. Eng. Educ. 34 (4) (1997) 331–337.
[39] M.A. Al-Alaoui, A class of second-order integrators and low-pass differentiators, IEEE Trans. Circuit. Syst. I 42 (4) (1995) 220–223.
[40] D.W. Jordan, P. Smith, Nonlinear ordinary differential equations: an introduction to dynamical systems, 2, Oxford University Press, USA, 1999.
[41] J. Klafter, S. Lim, R. Metzler, Fractional Dynamics: Recent Advances, World Scientific, 2012.
[42] M.S. Tavazoei, M. Haeri, A note on the stability of fractional order systems, Math. Comput. Simul. 79 (5) (2009) 1566–1576.
[43] J.-G. Lu, G. Chen, Robust stability and stabilization of fractional-order interval systems: an lmi approach, IEEE Trans. Autom. Control 54 (6) (2009) 1294–1299.
[44] A. Shilnikov, M. Kolomiets, Methods of the qualitative theory for the hindmarsh–rose model: a case study–a tutorial, Int. J. Bifurc. Chaos 18 (8) (2008) 2141–2168.
[45] H. Shou-Fang, Z. Ji-Qian, D. Shi-Jiang, State-to-state transitions in a Hindmarsh–Rose neuron system, Chin. Phys. Lett. 26 (5) (2009) 50502.